ORIGINAL SCIENTIFIC PAPER

CROATICA CHEMICA ACTA

Croat. Chem. Acta **2025**, *98*(2), 145–156
Published online: August 31, 2025
DOI: 10.5562/cca4172

HKD 1926

Gold Nanoparticles Functionalized with Peptidoglycan Monomer and 1-Adamantylamine Protect Dopaminergic Neurons Against Oxidative Damages Induced by L-Dopa

Ivan Mamić,[1] Maja Beus,[2] Nikolina Kalčec,[2] Nikolina Peranić,[2] Ruža Frkanec,[3] Petra Turčić,[1,*] Ivana Vinković Vrček[2,#]

[1] University of Zagreb, Faculty of Pharmacy and Biochemistry, A. Kovačića 1, 10000 Zagreb, Croatia
[2] Institute for Medical Research and Occupational Health, Ksaverska cesta 2, 10000 Zagreb, Croatia
[3] University of Zagreb, Centre for Research and Knowledge Transfer in Biotechnology, Rockfellerova 10, 10000 Zagreb, Croatia
* Corresponding author's e-mail address: pturcic@pharma.hr
# Corresponding author's e-mail address: ivinkovic@imi.hr

RECEIVED: April 1, 2025 * REVISED: June 24, 2025 * ACCEPTED: June 25, 2025

PROCEEDING OF THE SOLUTIONS IN CHEMISTRY 2024, 11–15 NOVEMBER 2024, SVETI MARTIN NA MURI, CROATIA

Abstract: Parkinson's disease (PD) is progressive neurodegenerative disorder marked by a loss of dopaminergic neurons, inflammation and oxidative stress and most commonly treated with L-Dopa. Long-term use of L-Dopa is associated with motor complications and side effects, highlighting the need for improved formulations. Gold nanoparticles (AuNPs) represent promising nanocarriers for improving drug delivery and reducing drug-induced toxicity. Building upon our previous work, where we demonstrated reversible binding of L-Dopa by AuNPs functionalized with peptidoglycan monomer (PGM-AuNPs) or 1-adamantylamine (Ad-AuNPs), we present here the intracellular uptake, biocompatibility, and antioxidative potential of such nanoformulations in vitro, using SH-SY5Y cells differentiated in dopaminergic neurons. Both AuNPs showed good biocompatibility, and no cytotoxicity at the tested concentrations. Intracellular uptake of AuNPs was confirmed using flow cytometry and confocal microscopy, with greater internalization seen for PGM-AuNPs compared to Ad-AuNPs. Finally, both AuNPs demonstrated the antioxidative effect under L-Dopa induced stress. These findings suggest that PGM- and Ad-AuNPs hold potential as effective nanocarriers while reducing L-Dopa induced oxidative stress.

Keywords: Parkinson`s disease, gold nanoparticles, nanocarriers, L-Dopa, SH-SY5Y.

INTRODUCTION

PARKINSON'S disease (PD) is the world's second most common neurodegenerative disorder, affecting roughly 1 % of people over the age of 60.[1] Despite significant scientific efforts, current pharmacological treatment is exclusively symptomatic. Despite being the most effective treatment for PD, chronic L-Dopa therapy is associated with debilitating motor complications leaving patient without effective treatment options.[2] Mechanism behind L-Dopa induced dyskinesias are poorly understood, but involve dopaminergic cell loss and consequential dopamine depletion, which remodels synapses in a way that pulsatile L-Dopa stimulation produces abnormal ganglia output.[3] In addition, some studies suggest that L-Dopa can contribute to oxidative stress,[4–6] excitotoxicity,[7] impairment of mitochondrial function,[8] thereby contributing to dopaminergic neuron degeneration. This emphasises the need for novel formulations that may minimize drug fluctuations and toxicity.

Nano-enabled drug delivery systems hold promises to address the limitations of conventional L-Dopa therapy.[9] Nanocarriers can be engineered to improve the pharmacokinetic profiles of the drugs, increase transport across biological barriers, protect the drug from peripheral metabolism and to enable targeted delivery. Among many nanomaterials, gold nanoparticles (AuNPs) are interesting due to their chemical inertness, biocompatibility, and simple synthesis.[10] They can be easily functionalized with targeting or transport-enhancing ligands, or loaded with

drugs.[11] AuNPs also exhibit intrinsic "nanozyme" activity that can either generate or scavenge reactive oxygen species (ROS): by carefully optimising their size, shape, and surface coating, these properties can be engineered to promote ROS formation for cancer therapy or to scavenge ROS and alleviate oxidative stress.[12] Aligned to their nanozyme properties, some studies even suggest AuNPs can restore impaired NAD+/NADH ratio in the brain of PD patients.[13] Finally, several clinical trials are currently evaluating AuNPs for therapeutic and diagnostic applications.[14] All of this makes AuNPs a promissing platform for the treatment of Parkinson`s disease.

In this study, we build upon our previous findings demonstrating that gold nanoparticles (AuNPs) functionalized with peptidoglycan monomer (PGM-AuNPs) or 1-adamantylamine (Ad-AuNPs) reversibly bind L-Dopa.[15] Here, we further investigate these AuNP-based formulations by assessing their intracellular uptake, effects on cell viability and oxidative stress, as well as evaluating their potential protective properties against L-Dopa-induced cytotoxicity under *in vitro* settings.

EXPERIMENTAL

AuNP Synthesis

PGM-AuNPs and Ad-AuNPs were synthesized using a reduction method as previously described.[15] Briefly, to obtain Ad-AuNP and PGM-AuNP, 10 mM $HAuCl_4 \cdot 3H_2O$ (Sigma-Aldrich, Chemie, GmbH) and 0.67 mM 1-adamantylamine hydrochloride (Sigma-Alrdich Chemie GmbH) or 0.12 mM PGM (Pliva, Chemical and Pharmaceutical Works, Zagreb, Croatia) were added to 6.5 mL of ultrapure water (UPW), followed by the addition of 15 mM $NaBH_4$ (Alfa Aesar, Kandel, Germany) under rigorous stirring. When the colour of the mixture turned from pale yellow to wine red it was stirred at room temperature for an additional 1.5 hours in the case of Ad-AuNPs and 20 minutes in the case of PGM-AuNPs. AuNPs were then purified by centrifugation at 8 000 × *g* 2 times for 10 min, respectively. The supernatant was removed, the pellet was resuspended in UPW and stored in the dark at 4 °C.

AuNPs Characterization

Detailed characterization of prepared AuNPs has been described in our previously published paper[15] and includes various spectroscopic, light scattering and microscopic techniques. Briefly, the elemental gold (Au) concentration of AuNP in stock suspension was determined using a graphite furnace atomic absorption spectrometer (GFAAS) (Perkin Elmer AAnalyst 600, Perkin Elmer, Shelton, USA) calibrated with a standard Au solution (1000 mg L^{-1} in 5 % HNO_3; Darmstadt, Germany) Method details along with calibration curves are available as supporting information (Figure S5, Table S1). Working concentrations for all biological experiments were prepared by diluting characterized stock suspension to desired final concentrations. The hydrodynamic diameter (d_H) and zeta (ζ) potential of AuNPs were determined from by dynamic (DLS) and electrophoretic light scattering (ELS) methods, respectively, using a Zetasizer Nano ZS (Malvern Instruments, Malvern, UK) equipped with a "green" laser (532 nm). DLS results were reported from the size-intensity distribution function as a mean value of six measurements with standard deviation, while ζ potential was calculated using Henry's equation with the Smoluchowski approximation and was expressed as the average value of six consecutive measurements with SD. Further characterization was performed using transmission electron microscopy (TEM, 902A; Carl Zeiss Meditec AG, Jena, Germany) in a bright-field mode with an acceleration voltage of 80 kV to determine the primary size (d_{TEM}) and shape of AuNPs. Additionally, AuNPs colloidal stability was assessed in UPW and complete cell culture medium using DLS and ELS techniques.

Calculation of Effective AuNP Exposure Concentrations

Besides reporting the nominal AuNPs concentrations (e.g., μg Au mL^{-1}) used in our experiments, we also estimated the actual dose delivered to the cell surface using the freely available "*in vitro* dosimetry" web application, which implements the distorted-grid model, as described by Cheimarios et al.[16] nanoparticles tend to agglomerate and sediment under standard cell culture conditions, the true concentration reaching cells can be substantially different than the nominal dose, which makes it difficult to accurately compare effects of two or more nanoparticle types, even when they have similar physicochemical properties. To calculate effective concentrations, we entered the nominal dose, DLS-derived volume-weighted size distributions, solvent properties, liquid height, effective density, and ran simulations for 4 h (related to oxidative stress assays) or 24 h (related to viability and uptake assays). We extracted the predicted particle concentration in the bottom 0.005 mm compartment — which accounts for sedimentation and diffusion — and used these effective doses alongside nominal concentrations when presenting our results. Effective concentrations are expressed as number of AuNPs per volume in the bottom compartment [N cm^{-3}].

Drug Loading Efficiency

To determine drug loading efficiency (DLE), AuNPs were incubated with L-Dopa in UPW for 10, 30, and 120 minutes. After incubation, free L-Dopa was separated from AuNPs on Amicon Ultra-2 Centrifugal Filter Unit (cut-off size 2 kDA, Merck, Darmstadt, Germany) at 3500 x *g* for 15 minutes.

The concentration of free L-Dopa in the ultrafiltrate was measured using a CARY 3500 UV-Vis spectrophotometer (Agilent Technologies, Santa Clara, USA) at a wavelength of 280 nm in a quartz cuvette with a 10 mm optical path length. A fresh standard calibration curve of L-Dopa (Figure S4) in UPW was prepared for each experiment and used to calculate the concentration of L-Dopa in the ultrafiltrate. DLE was calculated with the following equation:

$$DLE / \% = \left(\frac{\text{total amount of L-Dopa}}{\text{total amount of drug}} - \frac{\text{amount of free L-Dopa}}{\text{total amount of drug}} \right) * 100 \quad (1)$$

Cell Culture

SH-SY5Y cells (ECACC, Salisbury, UK) were grown in complete cell culture medium (CCM) composed of Dulbecco's Modified Eagle Medium/Nutrient Mixture F-12 (DMEM/F12), with 10 % fetal bovine serum (FBS), 1 % Penicillin/Streptomycin, 1 % non-essential-amino-acids, and 1 % L-glutamine (all purchased from Sigma-Aldrich Chemie GmbH, Germany). Cells were kept in T-75 culture flasks (Sarstedt, Nümbrecht, Germany) under humified conditions at 37 °C and 5 % CO_2. The medium was changed every four days and cells were subcultured when 70–80 % confluent. During subculturing, non-adherent cells were spun down and combined with adherent cells that were detached using 0.25 % Trypsin-EDTA solution (Sigma-Aldrich, Chemie GmbH). Cells were counted on TC20 Cell Counter (Bio-Rad, Hercules, USA). In all experiments cells between 5th and 15th passage were used. SH-SY5Y cells were differentiated towards dopaminergic-like phenotype according to protocol described elsewhere.[17,18] After seeding in the complete culture medium, cells were allowed to attach overnight. Next day, culture medium was removed, cells were washed with phosphate-buffered saline (PBS) and incubated in culture medium with 10 µM retinoic acid (RA; Sigma-Aldrich, Chemie GmbH, Germany) for 3 days. Retinoic acid was handled in the dark and kept minimum time at the room temperature to prevent degradation.[19] After 3 days the medium was removed, cells were rinsed with PBS, and incubated in cell culture medium with 80 nM 12-O-tetradecanoyl-13-acetate (TPA; Sigma-Aldrich, Chemie GmbH, Germany) for 3 additional days.

MTS Assay

Effect of PGM-AuNPs and Ad-AuNPs on cell viability in differentiated SH-SY5Y cells was assessed using CellTiter 96® Aqueous Non-Radioactive Cell Proliferation Assay (Promega, Madison, WI, USA) following manufacturer instructions. SH-SY5Y cells were seeded clear in 96-well plate (Eppendorf, Hamburg, Germany) at a density of 12.5 × 10^4 cells cm^{-2}, differentiated according to the protocol described above, and exposed to 2-fold serial dilution of Ad-AuNPs and PGM-AuNPs suspensions at 37 °C and 5 % CO_2. Treatments were prepared as 10× working concentration in UPW and diluted directly in the well to 1× final concentration. AuNPs were vortexed for 30 seconds before preparing solutions and before cell treatment. For negative control, cells were incubated in complete cell culture medium with the addition of sterile UPW. 10 % dimethyl sulfoxide (DMSO) was used as positive control. After 24 h cells were washed three times with PBS and 100 µL of phenol red-free complete cell culture medium was added to each well followed by 20 µL of MTS / PMS solution (20 : 1). Plate was incubated for 2 h at 37 °C and 5 % CO_2. Following incubation, absorbance was measured at 490 nm using Victor 3 microplate reader (Perkin Elmer, Waltham, MA, USA). Results are expressed as the mean ± standard error of the mean (SEM) relative to the negative control. At least three independent experiments were performed in triplicate, and blank values were subtracted from all absorbance measurements.

Flow Cytometry Experiments

Since AuNPs can interfere with conventional spectrophotometric assays such as MTS,[20] cell viability results were confirmed using an Annexin V-FITC/propidium iodide (PI) kit (Bio-Rad Laboratories, Hercules, CA, USA) on a CytoFLEX SRT Benchtop Cell Sorter (Beckman Coulter, Brea, CA, USA). This method also allowed us to investigate the AuNPs toxicity mechanism and their relative uptake into differentiated SH-SY5Y cells. Cells were seeded in 24-well plates (Eppendorf, Hamburg, Germany) at a density of 15 × 10^4 cells cm^{-2} and left to attach overnight at 37 °C and 5 % CO_2. Cells were differentiated according to the protocol described above. All treatments were prepared as 10× working solutions in sterile UPW and diluted to 1× final concentration directly in the well. For negative control cells were incubated in CCM with addition of sterile UPW. AuNPs were vortexed for 30 seconds before preparing solutions and before cell treatment. 10 % DMSO was used as positive control. Treatments were added to CCM, and plates were incubated for 24 h at 37 °C and 5 % CO_2. After incubation supernatants were collected in designated tubes, cells were rinsed with sterile PBS, and detached from plate with 0.25 % Trypsin-EDTA solution. CCM was added to inhibit trypsin activity and cell suspension was mixed with corresponding supernatants and PBS washes. Finally, cells were stained according to instructions in Annexin V Assay Kit (Biorad, Hercules, California, USA) to determine relative ammounts of live, late apoptotic/dead and early apoptotic cells. Additionally, side scattered light intensity (SSC) of live cells, measured by flow cytometry, was used as an indicator

of AuNPs uptake because it correlates with cellular granularity, which increases when metallic NPs are internalized. By comparing the median SSC intensity between treated and untreated cells, we quantified relative uptake of AuNPs.[21,22] Samples were analysed on a CytoFLEX SRT Benchtop Cell Sorter device (Beckman Coulter, Crea, CA, USA). Results are expressed as the mean ± standard error of the mean (SEM) relative to the negative control. Three independent experiments were performed in triplicate, and blank values were subtracted from all absorbance measurements.

Visualization of AuNPs in cells

Differentiated SH-SY5Y cells (12.5×10^4 cells cm^{-2}) seeded onto coverslips in 24-well plates (Eppendorf, Hamburg, Germany) were treated for 24 h with freshly prepared suspensions of Ad-AuNP or PGM-AuNP (final concentration: 10 μg Au mL^{-1}). After three PBS washes, cells were fixed (4 % paraformaldehyde, 10 min), permeabilized (0.25 % Triton X-100, 15 min), blocked (10 % FBS with 0.1 % Tween-20, 90 min at 37 °C), and incubated with mouse monoclonal anti-β-tubulin antibody (1 : 200, Sigma-Aldrich) overnight at 4 °C. Next, cells were incubated with AlexaFluor®488 secondary antibody (2 μg mL^{-1}, Abcam, 2 h), and stained with phalloidin-FITC (1 μg mL^{-1}, Sigma-Aldrich Chemie GmbH, Taufkirchen, Germany). Finally, nuclei were labeled with Hoechst 33258 (10 μg mL^{-1}, Sigma-Aldrich Chemie GmbH, Taufkirchen, Germany). Coverslips were mounted with Fluoroshield (Sigma-Aldrich) and stored at –20 °C until imaging. Confocal microscopy (Leica TCS SP8 X) with reflectance contrast mode was used to confirm nanoparticle internalization through Z-stack images (4–7 per sample), processed with ImageJ software (University of Wisconsin, USA).

Oxidative Stress and Mitochondrial Membrane Potential Measurements

SH-SY5Y cells were seeded in black 96-well plates (Thermo Fisher Scientific, Waltham, MA, USA) at a density of 12.5×10^4 cells/well and incubated overnight at 37 °C in a 5 % CO_2 atmosphere to allow attachment. Following differentiation as previously described, cells were washed with PBS and treated with AuNPs and/or L-Dopa. All treatments were freshly prepared in UPW at 10× working concentrations, 30 min prior to cell exposure. Nanoparticle solutions were vortexed for 30 s before dilution and application to cells. Final well concentrations were: AuNPs, 10 μg Au mL^{-1}; L-Dopa, 50 μM; and AuNPs loaded with L-Dopa, 50 μM L-Dopa / 10 μg Au mL^{-1} AuNPs. These concentrations were selected based on preliminary oxidative stress and flow cytometry experiments, aiming to induce oxidative stress without significant cytotoxicity and to maintain physiologically relevant L-Dopa concentrations.[23] Negative control cells were incubated in CCM supplemented with sterile UPW, while positive control cells were exposed to 20 μM tert-butyl hydroperoxide (t-BHP).

To measure oxidative stress parameters, AuNPs were removed, cells washed three times with PBS and incubated (40 min, room temperature) with fluorescent probes diluted in PBS (containing Ca^{2+} and Mg^{2+} to prevent cell dettachment): 20 μM 2',7'-dichlorodihydrofluorescein diacetate (DCFH-DA, Sigma-Aldrich Chemie GmbH, Taufkirchen, Germany) for general ROS detection; 20 μM dihydroethidium (DHE, Sigma-Aldrich Chemie GmbH) for superoxide radicals; 50 μM monochlorobimane (mBCl, Fluka) for reduced glutathione; and 0.1 μM rhodamine 123 (Rh123, Sigma-Aldrich Chemie GmbH) for mitochondrial membrane potential measurement. After incubation, the culture medium was carefully aspirated, cells rinsed twice with PBS, and fluorescence was immediately measured on a Victor3 microplate reader (PerkinElmer, Waltham, MA, USA). Excitation/emission wavelengths were set at 485/535 nm for DCFH-DA, 380/460 nm for mBCl, 507/529 nm for Rh123, and 480/567 nm for DHE. Background fluorescence (blank) values were subtracted from all measurements. Results are expressed as mean ± SEM relative to negative controls from at three independent experiments performed in triplicate.

Statistical Analysis

Statistical analysis was performed using GraphPad Prism 8 (GraphPad Software, San Diego, CA, USA). Data were analyzed for statistical significance by one-way ANOVA followed by Dunnett's multiple comparisons test, comparing all groups to the control. Tukey's test was applied for comparisons between multiple groups. A p-value < 0.05 was considered statistically significant.

RESULTS AND DISCUSSION

AuNP Characterization

The primary size and shape of AuNPs were determined using TEM. Both Ad-AuNPs and PGM-AuNPs present homogeneous spherical structures with similar primary diameters of aproximately 24 nm. (Figure 1). The d_H and ζ potential values were measured using DLS and ELS, respectively, in both UPW and CCM (Table 1). The d_H for both AuNPs were larger than their primary sizes determined by TEM (d_{TEM}), which can be attributed to the formation of hydration shell.[24,25] The polidispersity indexes (PDI) in UPW were above 0.1, a treshold for monodisperse systems.[26] ζ potential values in UPW were similar for both AuNPs, around to –30 mV, indicating good colloidal stability.[27] In the CCM, d_H of Ad-AuNPs increased significantly at 0 h, with further increase at 4 h, and remained stable up to 24 h. The initial d_H of PGM-AuNPs in

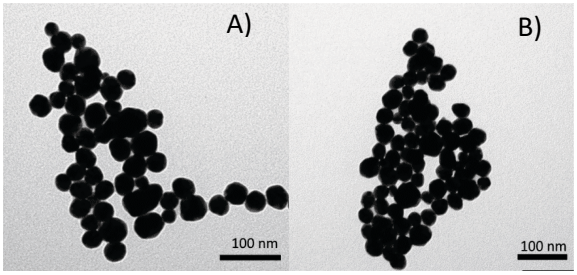

Figure 1. Transmission electron micrographs of gold nanoparticles (AuNPs) coated with A) 1-adamantylamine (Ad-AuNPs) and B) peptidoglycan monomer (PGM-AuNPs). Scale bars are 100 nm.

CCM was slghtly smaller compared to UPW, but increased substantially at 4 h and 24 h. The observed increase in d_H is likely due to the protein corona formation, rather than agglomeration, evidenced by stable PDI, monomodal intensity-weighted size distribution, and ζ potential values similar to those of serum proteins.[26,28,29] Protein corona likely stabilized the AuNPs in the CCM, despite ζ potential values not sufficient for electrostatic stabilization of nanoparticles.[27,30]

Drug Loading Efficiency

DLE analysis showed differences between Ad-AuNPS and PGM-AuNPS formulations (Table 2). PGM-AuNPS demonstated higher DLE than Ad-AuNPS at both tested concentrations (10 and 100 mg Au L^{-1}). At 100 mg Au L^{-1} and 500 µmol L^{-1} of L-Dopa, DLE for PGM-AuNPs was 10.3 ± 3.6 % after 10 min, increased to 11.1 ± 2.0 % after 30 min, and dropped slightly at 10.0 ± 2.0 % after 120 min. Under the same conditions, Ad-AuNPs performed poorer with 5.6 ± 3.1 % after 10 min, 5.9 ± 1.7 % after 30 min, and 3.9 ± 1.3 % after 120 min. At lower AuNPs and L-Dopa concentrations (10 mg Au L^{-1} and 50 µmol L^{-1}), results were similar, with PGM-AuNPs demonstrating better DLE. Since both of AuNPs have similar size, shape, surface charge, and total surface area, higher DLE exhibited by PGM-AuNPs is likely due to the more favorable surface chemistry.[31] DLE results were similar to our previously published work,[15] and aligned with usually reported DLE for nanoparticulate systems.[32] Since the highest DLE was observed after 30 min of incubation, this incubation time was selected for subsequent experiments involving L-Dopa-loaded AuNPs.

Table 1. Primary size (d_{TEM}, n = 100), hydrodynamic diameter (d_H), polydispersity index (PDI), and zeta potential (ζ) of gold nanoparticles (AuNPs) coated with 1-adamantylamine (Ad-AuNPs) and peptidoglycan monomer (PGM-AuNPs) in ultrapure water (UPW) and cell culture medium (CCM). Results are reported as mean values ± standard deviation.

AUNPs	d_{TEM} / nm			d_H / nm	ζ / mV	PDI
Ad-AuNPs	24.2 ± 2.9	UPW		85.6 ± 3.3	–29.3 ± 3.8	0.22
		CCM	0 h	111.4 ± 0.2	–11.2 ± 3.9	0.24
			4 h	124.6 ± 0.4	–15.1 ± 2.7	0.25
			24 h	125.1 ± 0.5	–13.3 ± 2.2	0.26
PGM-AuNPs	24.9 ± 3.4	UPW		79.3 ± 3.7	–31.2 ± 1.4	0.24
		CCM	0 h	74.1 ± 0.9	–9.5 ± 1.6	0.32
			4 h	81.9 ± 8.4	–11.6 ± 4.5	0.34
			24 h	97.1 ± 9.5	–13.6 ± 3.0	0.34

Cytotoxicity of AuNPs

MTS results showing cytotoxicity of PGM-AuNPs and Ad-AuNPs towards differentiated SH-SY5Y cells are given in Figure 2 After 24 h, none of the tested AuNPs concentrations showed significant cytotoxicity. Interestingly, at the highest AuNPs concentrations (100 and 200 µg Au mL^{-1}), viability values were significantly higher than negative

Table 2. Drug loading efficiency (DLE) of L-Dopa onto gold nanoparticles (AuNPs) functionalized with 1-adamantylamine (Ad-AuNPs) and peptidoglycan monomer (PGM-AuNsP). The AuNPs suspensions (10 and 100 mg Au/L) were incubated with L-Dopa (50 and 500 µmol L^{-1}, respectively), and samples were analyzed after 10, 30, and 120 min. DLE (%) is presented as mean ± standard deviation (SD) (n = 3). The table also includes AuNPs concentration given as number of nanoparticles per liter (N_{AuNP}/L), total nanoparticle surface area (SA, nm^2 L^{-1}), mass concentration (c_{Au} in mg Au L^{-1}), and L-Dopa molar concentration ($c_{L\text{-}Dopa}$ in µmol L^{-1}).

NP	c_{Au} / mg L^{-1}	c_{Au} / µmol L^{-1}	$c_{L\text{-}Dopa}$ / µmol L^{-1}	N_{AuNP} / L	total SA / nm^2 L^{-1}	10 min		30 min		120 min	
						DLE / %	SD	DLE / %	SD	DLE / %	SD
Ad-AuNP	100	507.7	500	6.98×10^{14}	1.28×10^{18}	5.6	3.1	5.9	1.7	3.9	1.3
	10	50.8	50	6.98×10^{13}	1.28×10^{17}	5.5	2.2	8.6	1.9	7.5	1.8
PGM-AuNP	100	507.7	500	6.4×10^{14}	1.24×10^{18}	10.3	3.6	11.1	2.0	10.0	2.0
	10	50.8	50	6.4×10^{13}	1.24×10^{17}	14.9	1.6	19.9	6.1	15.5	4.9

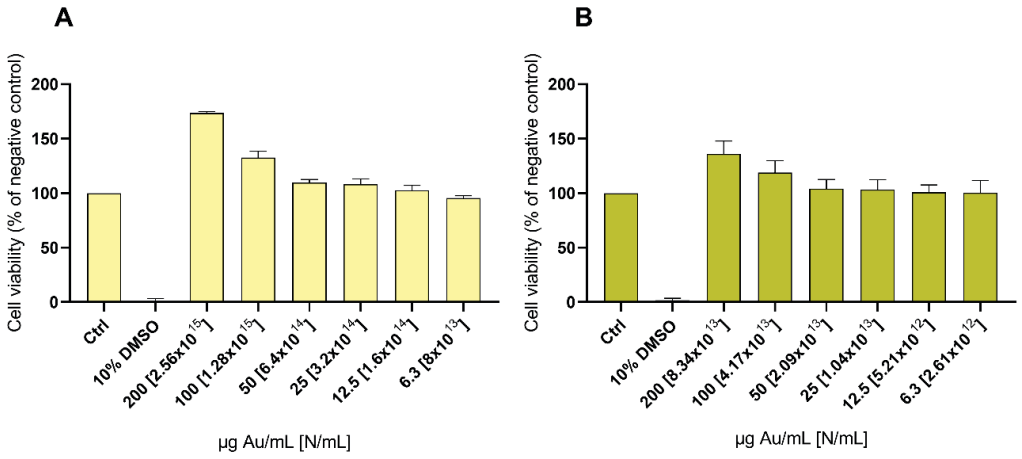

Figure 2. MTS assay results for peptidoglycan monomer (PGM-AuNPs, A) and 1-adamantylamine functionalized gold nanoparticles (Ad-AuNPs, B) after 24 h of treatment at 37 °C and 5 % CO_2. Untreated cells served as the negative control (Ctrl), while cells treated with 10 % dimethyl sulfoxide (10% DMSO) were used as the positive control. Data are presented as the mean percentage of control ± SEM (n = 4). Effective nanoparticle concentrations are indicated in the brackets.

control (Ctrl), which was probably caused by spectrophotometric interference induced by AuNPs,[33] since microscopic observations did not indicate toxicity, and AuNPs residues were clearly visible on the bottom of the wells even after extensive washing with PBS. Also, these AuNPs strongly absorb light around 500 nm,[15] which overlaps with detection wavelength of formazan. PGM-AuNPs seem to interfere more strongly, which may be due to 30-fold higher effective concentrations of PGM-AuNPs. Additionally, flow cytometry results did not demonstrate such artifact.

To confirm biocompatibility of AuNPs and evaluate their effect on induction of apoptosis, we employed Annexin V-FITC/PI assay using flow cytometry (Figure 3). Annexin V is protein that binds phosphatidyl serin,[34] which is translocated from inner to outer membrane in early apoptosis.[35] PI is membrane-impermeable dye that binds DNA, which happens upon membrane damage in late apoptotic cells or cells that undergo necrosis.[36] Based on this, it is possible to distinguish four different population of the cells: live (Annexin V-/PI-), dead (Annexin V-/PI+), early apoptotic (Annexin V+/PI-), and late apoptotic (Annexin V+/PI+).

At doses from 1 to 200 µg Au mL^{-1}, none of the AuNPs significantly affected number of live cells with all values above 80 % and comparable with the negative control (Figure 3A). Percentege of early apoptotic (Figure 3B), late apoptotic (Figure 3D), and dead cells (Figure 3C) also did not differ from negative control, while 10 % DMSO decreased the number of live cells to about 30 %. The same assays were used to evaluate L-Dopa toxicity (results presented in Figures S2 and S3 of Supporting Information).

Together, the MTS and flow cytometry results indicate no cytotoxicity at the tested AuNPs concentrations, confirming their biocompatibility.

The toxicity of AuNPs remains a subject of ongoing debate. While numerous studies report minimal or no toxicity at low-to-moderate concentrations, others found evidences of significant adverse effects.[37] For example, study by Valdiglesias et al.[38] demonstrated that negatively charged AuNPs (~5 nm) did not induce cell death in SH-SY5Y cells at concentrations up to 50 µg mL^{-1} after 24 hours. Similarly, a study on gold nanostars functionalized with polyethylene glycol (PEG) found no toxicity in SH-SY5Y cells at concentrations as high as 100 µg Au mL^{-1}. In contrast, gold nanostars functionalized with polyallylamine hydrochloride and PEG exhibited higher cellular uptake and clear dose-dependent cytotoxicity. Such findings highlight that AuNPs toxicity does not depend solely on nanoparticle composition but is strongly influenced by factors such as particle size, shape, and surface functionalization.[39–41] Therfore, it is wrong to just presume biocompatibility of AuNPs, but extensive toxicity screening is required to confirm it.

Although we tested a wide range of AuNPs concentrations and found no evidence of cytotoxcity, which is in line with most *in vitro* studies, possible adverse effects on human health outside this concentration range should be also considered. As mentioned above, the toxicological profile depends not only on dose but also on size, shape, surface modifications, route of administration, etc. This makes cross-study comparisons based solely on dose misleading.[42] Recent data suggest that concentrations below 1 µg mL^{-1} are generally well tolerated.[43–45] However, depending on the shape, size or surface charge AuNPs can

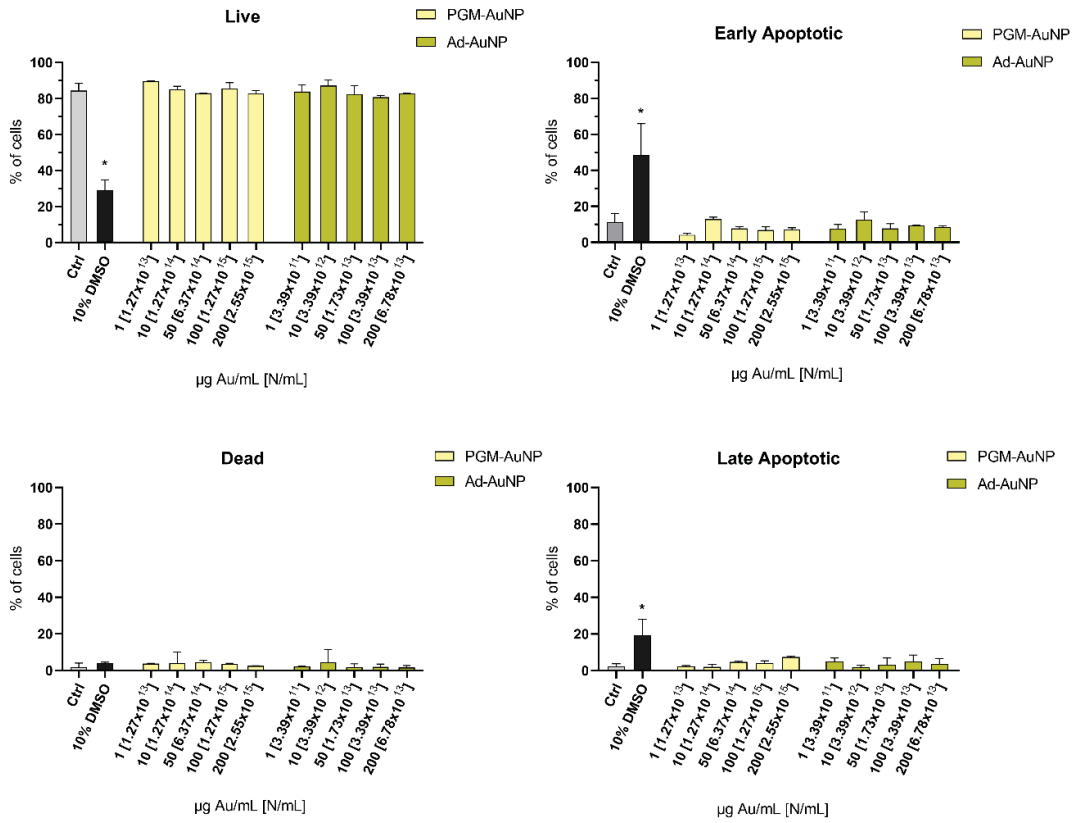

Figure 3. Effects of gold nanoparticles (AuNsP) functionalized with peptidoglycan monomer (PGM-AuNPs) and 1- adamantylamine (Ad-AuNPs) on differentiated SH-SY5Ycells. Cells were treated for 24 h at 37 °C and 5 % CO_2. Live cells; FITC-/PI-, early apoptotic: FITC+/PI-, late apoptotic FITC+/PI+, dead FITC-/PI+. Untreated cells served as the negative (Ctrl), while cells treated with 10 % DMSO were used as the positive control. Data were analyzed using one-way ANOVA, followed by Dunnett's multiple comparisons test against the control group. Results are expressed as mean ± SEM (n = 3). Asterisks (*) indicate statistically significant differences (p < 0.05). Effective AuNPs concentrations (N_{AuNPs} / mL) are given in the brackets.

exert toxicity even at doses below 1 µg mL^{-1}.[38,46,47] With increasing AuNP concentration, the classical "higher-dose → higher-risk" trend often holds, but even at doses above 100 µg mL^{-1}, outcomes remain formulation-specific: some NPs remain non-toxic.[48,49] and others induce nearly complete cell death.[50] Based on observed results, we may assume that toxicity with doses below tested is unlikely, while exposure to higher doses is also unlikely.

Besides short-term *in vitro* toxicity, a critical aspect of AuNPs` biocompatibility is the ability of AuNPs to accumulate inside the cells and organs. Such accumulation may lead to delayed or cumulative toxicity of non-toxic AuNPs doses and must be considered when developing Au-based nanodelivery systems. For example, the study by Liu Y et al.[51] demonstrated AuNPs accumulattion and cytotoxicity in TM3 cells in time- and concentration-dependent manner, with the most pronounced toxicity after 96 h incubation. The same study authors reported time-dependent accumulation of AuNPs inside the Leydig cells of BALB/c mice following 14-day intravenous injections. A study on BSA-coated AuNPs in mice revealed that AuNPs were still detectable in liver and spleen 120 days after a single intravenous injection accompanied by tissue inflammation and fibrosis.[52] Another *in vivo* study on AuNPs of various sizes clearly demonstrated that AuNPs between 8 and 37 nm in diameter induced toxicity with significant reduction in mice lifespan and sings of damage in the liver, lungs, and spleen.[53] These and similar studies underscore the limitations of short-term *in vitro* biocompatibility testing of AuNPs and confirm that *in vitro* results can not be translated to *in vivo.* Future work should focus on long-term, repeated dosing of AuNPs in animal models to determine AuNPs accumulation, biodistribution, and long-term safety profile of PGM- and Ad-AuNPs as potential L-Dopa delivery system.

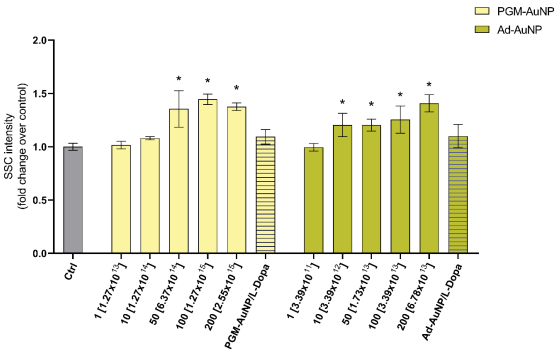

Figure 4. Uptake of Ad-AuNPs and PGM-AuNPs in dopaminergic neurons obtained from, differentiated SH-SY5Y cells as determined by side scatter light (SSC) intensity on flow cytometer. Cells were treated for 24 h at 37 °C and 5% CO_2. Untreated cells served as the control. For the combination group, L-Dopa (50 μm) was incubated with nanoparticles (10 μg Au mL^{-1}) for 30 min, followed by cell exposure. Data were analyzed by one-way ANOVA followed by Dunnett's multiple comparisons test versus control. Results are presented as mean ± SEM. Asterisks (*) indicate statistically significant difference ($p < 0.05$). Effective AuNPs concentrations are indicated in the brackets.

Our results clearly show that Ad-AuNPs and PGM-AuNPs are not toxic to *in vitro* model of the dopaminergic neurons at any tested concentration, indicating their good biocompatibility.

Nanoparticle Uptake by Dopaminergic Neurons

SSC intensity of the live cell population (PI-/Annexin V-FITC-) revealed a dose dependant uptake of AuNPs (Figure 4). At dose of 10 mg Au L^{-1}, uptake was poor for both AuNPs, and only slightly higher for Ad-AuNPs compared to PGM-AuNPs (1.15 vs 1.11). At doses above 10 μg Au mL^{-1} PGM-AuNPs were internalized more readily compared with Ad-AuNPs. This higher internalization could be due to the an order of magnitude higher effective concentration of PGM-AuNPs compared with Ad-AuNPs. Loading AuNPs with L-Dopa did not alter their uptake significantly.

Since flow cytometry cannot distinguish between internalized nanoparticles and those adsorbed on the cell surface,[54] confocal microscopy in reflectance mode was used to accurately determine AuNPs internalization.[55] Confocal images (Figures 5 and S1 in Supporting Information) and Z-stack videos (see Supporting Information) confirmed that AuNPs are present inside the dopaminergic neurons, with only rare instances of nuclear localization. This findings is expected since only very small AuNPs, with size usually bellow 10 nm, demonstrate efficient nuclear uptake.[56]

Oxidative Stress Response

One of the main mechanism behind AuNPs toxicity include oxidative stress, and inflammation, although pathways involved are usually complex.[37,57] Many studies link AuNPs to elevated ROS levels in cells. For example, a study by Zhang et al.[58] found that 4.5 nm PEG-coated AuNPs induced 6-fold increase in ROS levels in SH-SY5Y cells. This was accompanied by doubling of MDA, lipid peroxidation and mitochondrial damage. In PC12 cells, AuNPs induced high levels of ROS along with the cell death. The same study demonstrated coated AuNPs were more toxic compared to uncoated ones. However, comprehensive review on AuNP toxicity clearly stated that these response are dependent on physicochemical characteristics of AuNPs and that

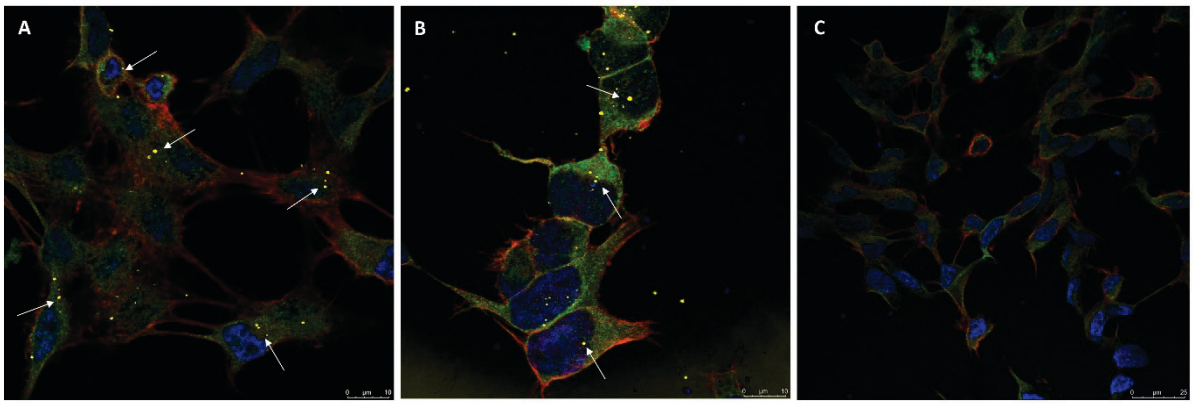

Figure 5. Confocal microscopy images of differentiated SH-SY5Y cells treated with Ad-AuNPs (A) and PGM-AuNPs (B) and non-treated control cells (C). All AuNPs were applied at a dose of 10 μg Au mL^{-1} and were visualized as yellow dots in the contrast reflectance channel of confocal microscope. Cell nuclei are stained blue, actin fibres red, and β-tubulin green (as shown in the composites of individual channels). White arrows indicate AuNPs inside the cell.

responses range from minimal to significant toxicity,[37] emphasiszing once again the need for thoroguh safety assesment of AuNPs, despite existing body of literature supports their biocompatibility.

We evaluated oxidative stress response in dopaminergic neurons by means of mitochondrial membrane potential, ROS and GSH levels. ROS levels in differentiated SH-SY5Y cells were quantified with 2,7-dichlorofluorescin diacetate (DCFH-DA) and dihydroethidium (DHE) assays (Figures 6A and B). After 4 h of treatment, t-BHP and L-Dopa increased DHE fluorescence intensity relative to control by 1.12 and 1.29, respectively, indicating production of ROS. AuNPs alone did not induce ROS production and more importantly attenuated effects of L-Dopa as evidenced by decrease in fluorescence intensity from 1.29 to 0.91 for L-Dopa loaded to PGM-AuNPs and 0.96 for L-Dopa loaded to Ad-AuNPs.

GSH levels were assessed using mBCL assay (Figure 6C). L-Dopa reduced GSH levels to 0.79 relative to control, while none of the AuNPs alone had significant effect on GSH levels at a dose of 10 μg Au mL^{-1}. When combined with L-Dopa, PGM-AuNP and Ad-AuNP were able to maintain higher levels of GSH compared with L-Dopa treatment alone (0.86 and 0.97), but none of the results are statistically significant.

Mitochondrial membrane potential was evaluated using Rh123 staining (Figure 6D). L-Dopa reduced mitochondrial membrane potential as evidenced by decrease in

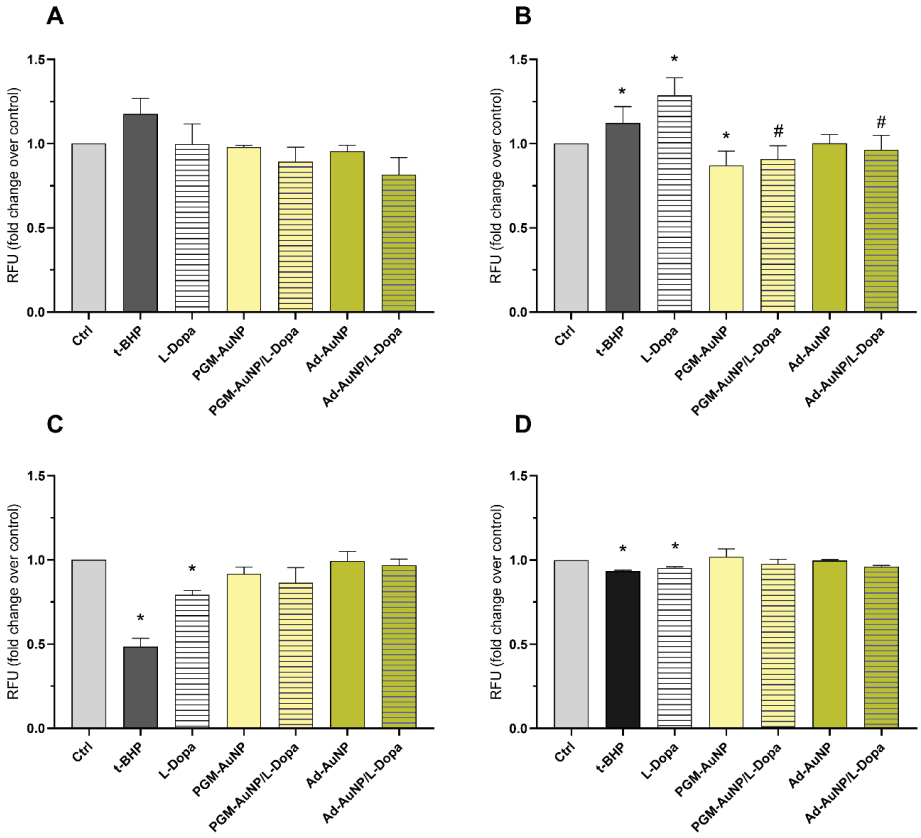

Figure 6. Effects of gold nanoparticles (AuNPs) on the generation of reactive oxygen species (A; DCFH2-DA assay), superoxide radicals (B; DHE assay), intracellular reduced glutathione levels (C; mBCL assay), and mitochondrial membrane potential (D; Rh123 assay) in differentiated SH-SY5Y cells after a 4-hour treatment at 37 °C and 5 % CO_2. Cells were treated with either peptidoglycan monomer-functionalized AuNPs (PGM-AuNPs) or 1-adamantylamine-functionalized AuNPs (Ad-AuNPs) at 10 μg Au mL^{-1}, or with AuNPs pre-loaded with L-Dopa (50 μM L-Dopa / 10 μg Au mL^{-1}). Corresponding AuNPs effective concentrations were 1.27×10^{14} and 2.98×10^{12}. Untreated cells served as the negative control (Ctrl), whereas cells exposed to 20 μM tert-butyl hydroperoxide (tBHP) were used as the positive control. Results are presented as mean fold-change relative to control ± SEM (n = 3). Statistical analysis was conducted using one-way ANOVA followed by Tukey's multiple comparisons test. Significant differences ($p < 0.05$) are indicated with an asterisk (*) versus the vehicle control (VC) and a hash (#) versus the L-Dopa-treated group (LD).

Rh123 dye fluorescence. PGM-AuNP and Ad-AuNP had negligible effects on mitochondrial membrane potential with relative fluorescence values of 1.02 and 1.00, respectively. When combined with L-Dopa, AuNPs increased Rh123 fluorescence compared to L-Dopa alone, suggesting protective effects, but the results were not statistically significant.

These results indicate that PGM-AuNPs and Ad-AuNPs did not impair mitochondrial function or increased ROS levels at selected concentrations. Furthermore, they effectively attenuated L-Dopa-induced ROS production, GSH depletion, and mitochondrial membrane potential reduction in differentiated SH-SY5Y cells, although not all results were statistically significant.

The protective effects observed in this study could be due to reduction in free L-Dopa concentration, AuNPs "nanozyme" activity, or free radical scavenging ability of AuNPs.[59,60] Other mechanisms may also play a role; but the assays used in this study do not allow for their identification. Further research should therefore focus more on elucidating underlying antioxidative pathways as this is essential for the design of more effective nano-enabled drug carriers.

Finally, when interpreting the results, the potential for AuNP interferences with conventional assays should be considered as they represent a great challenge in nanotoxicology research and often lead to data misinterpretation.[61,62] The AuNPs used in this study have absorption peak around 500 nm, which may overlap with the emission wavelengths of fluorescent probes and cause signal attenuation. AuNPs can also scatter visible light and due to their surface plasmon resonance properties they can either enhance or quench fluorescent signals from assays like mBCL, Rh123, and DHE. In our study, we used relatively low AuNPs concentrations along with multiple washing steps to remove unbound particles prior to dye incubation and fluorescence measurement. Furthermore, consistency across different assays suggests that obtained results reflect true biological response rather than artifacts arising from nanoparticle-induced interferences.

Taken together, the results presented in this study demonstrate the potential of PGM- and Ad-AuNPs as L-Dopa carriers, but validation in *in vivo* models is necessary not only to confirm these findings, but also to expand on important aspects like pharmacokinetics, which cannnot be tested *in vitro.* Such next studies require careful planning and execution, since *in vivo* testing is complex, costly and time consuming, requires trained personnel, long-term dosing regimens, and must comply with high ethical standards. *In vivo* testing of nanomaterials comes with some specific challenges like lack of standardised assays and protocols, difficulties in scaling up nanoparticle production, and batch to batch variability.[63] On the end note, results obtained on animal models can be difficult to translate to humans due to the species-related differences in physiology.

CONCLUSION

This study provides evidence that PGM-AuNPs or Ad-AuNP are biocompatible carriers of L-Dopa and reduce L-Dopa-induced oxidative damage in an a *in vitro* model of dopaminergic neurons. None of AuNPs showed cytotoxicity at the tested concentrations, assessed by MTS and flow cytometry assays. Cellular uptake studies suggest higher internalization of PGM-AuNPs compared to Ad-AuNPs, which may be due to their greater effective concentrations. Interestingly, both AuNP formulations were able to alleviate L-Dopa-induced oxidative stress. The results suggest that functionalized AuNPs can serve as carriers of L-Dopa and simultaneously exert protective effects against drug-induced toxicity in the model of dopaminergic neurons. Future studies should focus on more advanced models to validate these results.

Acknowledgment. This study was financially supported by the "Research Cooperability" Program of the Croatian Science Foundation funded by the European Union from the European Social Fund under the Operational Programme Efficient Human Resources 2014 – 2020 (grant HRZZ-PZS-2019-02-4323), by the European Regional Development Fund project KK.01.1.1.02.0007 "Research and Education Centre of Environmental Health and Radiation Protection – Reconstruction and Expansion of the Institute for Medical Research and Occupational Health" and the European Union – Next Generation EU programme (contract document designation 643-02/23-01/00016).

Supplementary Information. Supporting information to the paper is attached to the electronic version of the article at: https://doi.org/10.5562/cca4172.

PDF files with attached documents are best viewed with Adobe Acrobat Reader which is free and can be downloaded from Adobe's web site.

REFERENCES

[1] O.-B. Tysnes, A. Storstein, *J. Neural Transm.* **2017**, *124*, 901–905. https://doi.org/10.1007/s00702-017-1686-y

[2] J. E. Ahlskog, M. D. Muenter, *Mov. Disord. Off. J. Mov. Disord. Soc.* **2001**, *16*, 448–458.

[3] P. Jenner, *Nat. Rev. Neurosci.* **2008**, *9*, 665–678. https://doi.org/10.1038/nrn2471

[4] T. Alexander, C. E. Sortwell, C. D. Sladek, R. H. Roth, K. Steece-Collier, *Cell Transplant.* **1997**, *6*, 309–317. https://doi.org/10.1177/096368979700600313

[5] C. T. Lai, P. H. Yu, *Biochem. Pharmacol.* **1997**, *53*, 363–368. https://doi.org/10.1016/S0006-2952(96)00731-9

[6] N. Nakao, K. Nakai, T. Itakura, *Brain Res.* **1997**, *777*, 202–210. https://doi.org/10.1016/S0006-8993(97)01116-5
[7] E. Guatteo, A. Yee, J. McKearney, M. L. Cucchiaroni, M. Armogida, N. Berretta, N. B. Mercuri, J. Lipski, *Exp. Neurol.* **2013**, *247*, 582–590. https://doi.org/10.1016/j.expneurol.2013.02.009
[8] P. Hörmann, S. Delcambre, J. Hanke, R. Geffers, M. Leist, K. Hiller, *Cell Death Discov.* **2021**, *7*, 151. https://doi.org/10.1038/s41420-021-00547-4
[9] T. M. Sim, D. Tarini, S. T. Dheen, B. H. Bay, D. K. Srinivasan, *Int. J. Mol. Sci.* **2020**, *21*, 6070. https://doi.org/10.3390/ijms21176070
[10] M. Kus-Liśkiewicz, P. Fickers, I. Ben Tahar, *Int. J. Mol. Sci.* **2021**, *22*, 10952. https://doi.org/10.3390/ijms222010952
[11] S. J. Amina, B. Guo, *Int. J. Nanomedicine* **2020**, *15*, 9823–9836. https://doi.org/10.2147/IJN.S279094
[12] J. Lou-Franco, B. Das, C. Elliott, C. Cao, *Nano-Micro Lett.* **2020**, *13*, 10. https://doi.org/10.1007/s40820-020-00532-z
[13] J. Ren, R. B. Dewey, A. Rynders, J. Evan, J. Evan, S. Ligozio, K. S. Ho, P. V. Sguigna, R. Glanzman, M. T. Hotchkin, R. B. Dewey, B. M. Greenberg, *J. Nanobiotechnology* **2023**, *21*, 478. https://doi.org/10.1186/s12951-023-02236-z
[14] L. Yao, D. Bojic, M. Liu, *J. Pharm. Anal.* **2023**, *13*, 960–968. https://doi.org/10.1016/j.jpha.2023.06.001
[15] N. Kalčec, N. Peranić, R. Barbir, C. R. Hall, T. A. Smith, M. A. Sani, R. Frkanec, F. Separovic, I. Vinković Vrček, *Spectrochim. Acta. A. Mol. Biomol. Spectrosc.* **2022**, *268*, 120707. https://doi.org/10.1016/j.saa.2021.120707
[16] N. Cheimarios, B. Pem, A. Tsoumanis, K. Ilić, I. V. Vrček, G. Melagraki, D. Bitounis, P. Isigonis, M. Dusinska, I. Lynch, P. Demokritou, A. Afantitis, *Nanomaterials* **2022**, *12*, 3935. https://doi.org/10.3390/nano12223935
[17] S. P. Presgraves, T. Ahmed, S. Borwege, J. N. Joyce, *Neurotox. Res.* **2003**, *5*, 579–586. https://doi.org/10.1007/BF03033178
[18] S. Påhlman, A.-I. Ruusala, L. Abrahamsson, M. E. K. Mattsson, T. Esscher, *Cell Differ.* **1984**, *14*, 135–144. https://doi.org/10.1016/0045-6039(84)90038-1
[19] K. A. Sharow, B. Temkin, M. A. Asson-Batres, *Int. J. Dev. Biol.* **2012**, *56*, 273–281. https://doi.org/10.1387/ijdb.113378ks
[20] I. V. Vrček, I. Pavičić, T. Crnković, D. Jurašin, M. Babič, D. Horák, M. Lovrić, L. Ferhatović, M. Ćurlin, S. Gajović, *RSC Adv.* **2015**, *5*, 70787–70798. https://doi.org/10.1039/C5RA14100A
[21] H. Suzuki, T. Toyooka, Y. Ibuki, *Environ. Sci. Technol.* **2007**, *41*, 3018–3023. https://doi.org/10.1021/es0625632
[22] R. M. Zucker, K. M. Daniel, E. J. Massaro, S. J. Karafas, L. L. Degn, W. K. Boyes, *Cytom. Part J. Int. Soc. Anal. Cytol.* **2013**, *83*, 962–970. https://doi.org/10.1002/cyto.a.22342
[23] J. Lipski, R. Nistico, N. Berretta, E. Guatteo, G. Bernardi, N. B. Mercuri, *Prog. Neurobiol.* **2011**, *94*, 389–404. https://doi.org/10.1016/j.pneurobio.2011.06.005
[24] R. Pecora, *J. Nanoparticle Res.* **2000**, *2*, 123–130. https://doi.org/10.1023/A:1010067107182
[25] J. Jiang, G. Oberdörster, P. Biswas, *J. Nanoparticle Res.* **2009**, *11*, 77–89. https://doi.org/10.1007/s11051-008-9446-4
[26] P. Eaton, P. Quaresma, C. Soares, C. Neves, M. P. de Almeida, E. Pereira, P. West, *Ultramicroscopy* **2017**, *182*, 179–186. https://doi.org/10.1016/j.ultramic.2017.07.001
[27] O. Z. Sharaf, R. A. Taylor, E. Abu-Nada, *Phys. Rep.* **2020**, *867*, 1–57. https://doi.org/10.1016/j.physrep.2020.04.005
[28] I. Capjak, S. Š. Goreta, D. D. Jurašin, I. V. Vrček, *Arch. Ind. Hyg. Toxicol.* **2017**, *68*, 245–253. https://doi.org/10.1515/aiht-2017-68-3054
[29] S. R. Saptarshi, A. Duschl, A. L. Lopata, *J. Nanobiotechnology* **2013**, *11*, 26. https://doi.org/10.1186/1477-3155-11-26
[30] A. A. Cohen, K. Shemesh, R. Gur, *Front. Cell. Neurosci.* **2021**, *15*, 715449. https://doi.org/10.3389/fncel.2021.715449
[31] M. Nouri, M. E. Rezayat, M. G. H. Nouri, M. M. Pashaei, S. R. Abbasi, *Mol. Neurobiol.* **2017**, *54*, 1745–1756. https://doi.org/10.1007/s12035-016-9784-0
[32] R. M. Pinho, D. R. Paiva, L. B. Menezes, S. J. Monteiro, *Biochimie* **2021**, *186*, 101–110. https://doi.org/10.1016/j.biochi.2021.08.002
[33] G. Salama, A. G. Morsi, A. M. Ibrahim, S. M. Abdel-Rahman, *J. Mol. Neurosci.* **2019**, *69*, 553–559. https://doi.org/10.1007/s12031-019-01423-1
[34] G. G. Tiwari, P. D. Kumar, P. S. Singh, *J. Pharmacol. Exp. Ther.* **2013**, *346*, 200–207. https://doi.org/10.1124/jpet.113.205007
[35] M. P. Hejazi, A. Sadeghi, S. A. Darvish, *Neurotox. Res.* **2018**, *33*, 548–559. https://doi.org/10.1007/s12640-018-9885-5
[36] S. Zhu, L. Zhang, Y. Zhou, Z. Liu, H. Zhao, *Int. J. Mol. Sci.* **2020**, *21*, 4826. https://doi.org/10.3390/ijms21144826
[37] C. Gao, Z. Cao, Y. Zhao, J. Zhou, X. Wang, H. Wei, *Nanomaterials* **2022**, *12*, 1144. https://doi.org/10.3390/nano12071144

[38] F. I. Senthilkumar, M. Y. Jeong, J. H. Kim, S. S. Lee, *Toxicol. Res.* **2020**, *36*, 381–390. https://doi.org/10.1039/D0TX00018E
[39] Y. Wu, W. Wang, F. Chen, M. Sun, *J. Pharm. Sci.* **2021**, *110*, 3133–3141. https://doi.org/10.1016/j.xphs.2021.07.018
[40] M. Magro, D. Sgambato, A. Ingrassia, F. Di Salvo, *J. Trace Elem. Med. Biol.* **2016**, *37*, 60–67. https://doi.org/10.1016/j.jtemb.2016.05.009
[41] M. Wang, H. Qiu, H. Li, *J. Environ. Sci. (China)* **2018**, *67*, 90–99. https://doi.org/10.1016/j.jes.2017.07.009
[42] M. A. M. Silva, M. A. Camargo, *J. Appl. Toxicol.* **2019**, *39*, 763–771. https://doi.org/10.1002/jat.3757
[43] R. R. de Oliveira, G. C. R. de Oliveira, *Toxicol. Lett.* **2020**, *332*, 128–135. https://doi.org/10.1016/j.toxlet.2020.06.009
[44] P. Q. Nguyen, T. V. Hoang, *Nanotoxicology* **2021**, *15*, 1354–1365. https://doi.org/10.1080/17435390.2021.1921359
[45] M. A. Zaki, N. S. Mohamed, *J. Hazard. Mater.* **2022**, *429*, 128376. https://doi.org/10.1016/j.jhazmat.2021.128376
[46] C. F. Dias, M. V. Tavares, M. R. de Lima, A. P. C. Campos, *J. Pharm. Biomed. Anal.* **2019**, *171*, 312–320. https://doi.org/10.1016/j.jpba.2019.01.040
[47] Y. Wang, J. Zhang, X. Liu, *J. Controlled Release* **2017**, *261*, 85–95. https://doi.org/10.1016/j.jconrel.2017.07.020
[48] H. A. Hassan, F. M. Salem, *J. Pharm. Sci.* **2018**, *107*, 3447–3454. https://doi.org/10.1016/j.xphs.2018.05.022
[49] L. B. Al-Abd, A. M. Hegazy, M. H. Ibrahim, *Biomed. Pharmacother.* **2019**, *112*, 108703. https://doi.org/10.1016/j.biopha.2019.108703
[50] J. J. Zhang, L. L. Wang, *J. Nanobiotechnology* **2020**, *18*, 153. https://doi.org/10.1186/s12951-020-00681-7
[51] M. H. Al-Saleh, *Int. J. Mol. Sci.* **2021**, *22*, 1274. https://doi.org/10.3390/ijms22031274
[52] R. J. Nelson, C. J. Beuhler, *J. Environ. Sci. Health Part A* **2019**, *54*, 102–108. https://doi.org/10.1080/10934529.2018.1524193
[53] K. Zhang, J. Xu, F. Liao, *Int. J. Nanomedicine* **2017**, *12*, 5441–5452. https://doi.org/10.2147/IJN.S141410
[54] S. K. Singh, A. Kumar, R. Meena, *J. Toxicol. Sci.* **2020**, *45*, 33–41. https://doi.org/10.2131/jts.45.33
[55] Y. Y. Liu, H. B. Wu, *Sci. Total Environ.* **2021**, *755*, 143695. https://doi.org/10.1016/j.scitotenv.2020.143695
[56] J. M. Smith, R. C. Johnson, *Neurochem. Int.* **2018**, *117*, 1–9. https://doi.org/10.1016/j.neuint.2017.11.002
[57] P. R. Williams, L. M. Lee, *J. Neurosci. Methods* **2016**, *267*, 23–30. https://doi.org/10.1016/j.jneumeth.2016.06.012
[58] S. Y. Kim, H. S. Lee, *Brain Res. Bull.* **2019**, *147*, 89–95. https://doi.org/10.1016/j.brainresbull.2019.03.008
[59] D. P. Garcia, L. R. Torres, *Mol. Cell. Neurosci.* **2020**, *104*, 103468. https://doi.org/10.1016/j.mcn.2020.103468
[60] M. L. Gonzalez, S. R. Perez, *J. Neurochem.* **2017**, *141*, 724–732. https://doi.org/10.1111/jnc.14034
[61] F. T. Martin, A. G. Brown, *Neurosci. Lett.* **2015**, *594*, 45–50. https://doi.org/10.1016/j.neulet.2015.02.008
[62] R. J. Thompson, K. A. Hall, *J. Neurol. Sci.* **2019**, *406*, 45–51. https://doi.org/10.1016/j.jns.2019.05.017
[63] L. M. King, D. E. Walters, *Front. Neurosci.* **2023**, *17*, 1234. https://doi.org/10.3389/fnins.2023.01234